Available on the CERN CDS information server **CMS PAS SUS-12-018**

CMS Physics Analysis Summary

Contact: cms-pag-conveners-susy@cern.ch 2012/07/07

Search for Supersymmetry in Events with Photons and Missing Energy

The CMS Collaboration

Abstract

We have performed a search for beyond the standard model physics with photons and missing transverse energy. The data sample corresponds to an integrated luminosity of 4.04 fb^{-1} of pp collisions at $\sqrt{s} = 8$ TeV, recorded by the CMS experiment at the LHC. We compare the missing transverse energy distribution in events containing either at least two photons plus at least one hadronic jet or at least one photon plus at least two hadronic jets to the spectra expected from standard model processes. No excess of events at high missing transverse energy is observed, and results are interpreted in the context of General Gauge Mediated SUSY with the next to lightest SUSY particle being either a bino and wino-like neutralino. 95% confidence level upper limits on the signal production cross sections for different composition and decay modes of the SUSY particles are determined for a range of squark and gluino masses.

1 Introduction

Many beyond the standard model scenarios predict an excess in events with missing transverse energy above standard model predictions. Of these, supersymmetry (SUSY), in particular the version based on gauge-mediated SUSY breaking [1–7], is of high theoretical interest for physics beyond the standard model (SM). It stabilizes the mass of the SM Higgs boson, drives the grand unification of forces, and avoids the flavor problems endemic in other SUSY breaking scenarios. Models with universal extra dimensions may also lead to similar final state signatures.

This search is framed around a GGM SUSY scenario [8, 9], in which the gravitino ($\widetilde{\mathrm{G}}$) is the lightest SUSY particle (LSP) and the lightest neutralino ($\widetilde{\chi}_1^0$) is the next-to-lightest SUSY particle (NLSP). If the neutralino is contains a significant wino-like component, the lightest charginos become co-NLSP's. Assuming that R-parity [10] is conserved, strongly-interacting SUSY particles are predicted to be pair-produced at the LHC. Their decay chains would include one or several quarks and gluons, manifesting as jets in the detector. The decay cascades would end in the neutralino/chargino NLSP. If the neutralino composition is mostly bino-like it will decay predominantly to a photon and the gravitino LSP. The gravitino escapes detection, leading to missing transverse energy ($E_{\mathrm{T}}^{\mathrm{miss}}$) in the event. The two photons from the bino-like neutralinos motivate a search based on a pair of photons in the final state with $E_{\mathrm{T}}^{\mathrm{miss}}$. If the neutralino is wino-like, the neutralino would tend to decay to a Z and gravitino (charginos would decay to W and a gravitino). In this case the photon + gravitino decay mode is still available, albeit suppressed, motivating a search requiring only one photon associated with jets and $E_{\mathrm{T}}^{\mathrm{miss}}$. Long-lived neutralino scenarios (see e.g. Ref. [11]) are not covered in this analysis.

Searches for new physics with this signature were previously performed at ATLAS with 36 pb^{-1} [12] and 1.1 fb^{-1} [13] of pp collision data, CMS with 36 pb^{-1} [14], as well as the Tevatron [15, 16], LEP [17–20], and HERA [21]. The most recent CMS search [22] based on 4.7 fb^{-1} of data collected at $\sqrt{s} = 7$ TeV constrained the production of squarks and gluinos to masses above $\sim$ 800-1000 GeV based on a simplified model [23]. The other searches put constraints on the gauge boson partners, with the current best lower limit on the neutralino mass [16] of 175 GeV in a general gauge-mediation (GGM) SUSY scenario similar to what is studied here.

Table 1: Some general characteristics of the GGM cascades leading to the topologies of interest.

NLSP type	γ + 2 jets + $E_{\mathrm{T}}^{\mathrm{miss}}$	$\gamma\gamma$ + jet + $E_{\mathrm{T}}^{\mathrm{miss}}$
Bino	$\mathrm{jets} + \widetilde{\chi}_1^0\widetilde{\chi}_1^0 \to \mathrm{jets} + \gamma + Z + \widetilde{\mathrm{G}}\widetilde{\mathrm{G}}$	$\mathrm{jets} + \widetilde{\chi}_1^0\widetilde{\chi}_1^0 \to \mathrm{jets} + \gamma\gamma + \widetilde{\mathrm{G}}\widetilde{\mathrm{G}}$
Wino	$\mathrm{jets} + \widetilde{\chi}_1^0\widetilde{\chi}_1^0 \to \mathrm{jets} + \gamma + Z + \widetilde{\mathrm{G}}\widetilde{\mathrm{G}}$ $\mathrm{jets} + \widetilde{\chi}_1^0\widetilde{\chi}_1^\pm \to \mathrm{jets} + \gamma + W^\pm + \widetilde{\mathrm{G}}\widetilde{\mathrm{G}}$	$\mathrm{jets} + \widetilde{\chi}_1^0\widetilde{\chi}_1^0 \to \mathrm{jets} + \gamma\gamma + \widetilde{\mathrm{G}}\widetilde{\mathrm{G}}$

The two final state topologies studied in this search are:

- two (or more) isolated photons with transverse energy E_{T} above 40 and 25 GeV respectively, at least one hadronic jet, and large $E_{\mathrm{T}}^{\mathrm{miss}}$;
- at least one isolated photon with E_{T} above 80 GeV, at least two hadronic jets, and large $E_{\mathrm{T}}^{\mathrm{miss}}$.

In neither topology do we veto on the presence of isolated leptons, as especially in the wino co-NLSP case doing so would restrict the acceptance of the neutralino decays into Z and chargino decays into $W^\pm$ which could be present for sufficiently high neutralino masses. Table 1 gives example decay chains leading to these final states. The table is divided horizontally between

single-photon vs di-photon target final states. The vertical direction differentiates between bino NLSP and wino co-NLSP cases. The number of jets produced in the cascades can vary depending on whether gluinos or squarks are produced and the species of quarks in the final state. The jet multiplicity requirements in either analysis (one jet for diphoton, two jets for single photon) were chosen to be most inclusive over this full mass parameter space.

2 Data Selection

A detailed description of the CMS detector can be found elsewhere [24]. The detector's central feature is a superconducting solenoid providing a 3.8 T axial magnetic field along the beam direction. Charged particle trajectories are measured by a silicon pixel and strip tracker system, covering $0 \leq \phi \leq 2\pi$ in azimuth and $|\eta| < 2.5$, where the pseudorapidity $\eta = -\ln[\tan\theta/2]$, and θ is the polar angle with respect to the counterclockwise beam direction. A lead-tungstate crystal electromagnetic calorimeter (ECAL) and a brass/scintillator hadron calorimeter (HCAL) surround the tracker volume. For the barrel calorimeter ($|\eta| < 1.479$), the modules are arranged in projective towers. Muons are measured in gas ionization chambers embedded in the steel return yoke of the magnet. The detector is nearly hermetic, allowing for reliable measurement of $E_{\mathrm{T}}^{\mathrm{miss}}$. In the 2011 collision data, unconverted photons with energy greater than 30 GeV are measured within the barrel ECAL with a resolution of better than 1% [25], which is dominated by inter-calibration precision.

The data used in this analysis were recorded during the 2012 LHC run and corresponds to an integrated luminosity of 4.04 fb^{-1}. Events were recorded using the CMS two-level trigger system requiring the presence of at least one high-energy photon and significant hadronic activity or at least two photons. This data sample is utilized for the selection of both signal candidates and control samples used for background estimation. The particular triggers used for the single-photon and di-photon analyses are discussed below.

The photon candidates are reconstructed from clusters of energy in the ECAL. Candidate events are required to have at least one (two) photon(s) with a minimum transverse energy for the single-photon (di-photon) analysis. We require the ECAL cluster shape to be consistent with that expected from a photon, and the energy detected in HCAL behind the photon shower not to exceed 5% of the ECAL energy. To suppress hadronic jets giving rise to photon candidates, we require the latter to be isolated from other activity in the tracker, ECAL and HCAL. A cone of $\Delta R = \sqrt{(\Delta\eta)^2 + (\Delta\phi)^2} = 0.3$ is constructed around the candidates' direction, and the scalar sums of transverse energies of tracks and calorimeter deposits within this ΔR cone are determined, after excluding the contribution from the candidate itself. These isolation sums for the tracker, ECAL and HCAL are added and required to be less than 6 GeV after correcting for pile-up effects.

Photons that fail either the shower shape or track isolation requirement are referred to as *fake photons*. These objects are dominantly electromagnetically fluctuated jets and are used for the background estimation based on data.

The criteria above are efficient for the selection of both electrons and photons. To reliably separate them, we search for hit patterns in the pixel detector consistent with a track from an electron (pixel match). The candidates without pixel match are considered to be photons. Otherwise they are considered to be electrons, which we will use to select control samples for background estimation.

Jets and $E_{\mathrm{T}}^{\mathrm{miss}}$ are reconstructed with a particle-flow technique [26]. This algorithm reconstructs

all particles produced in the collision and subsequently identifies them as charged or neutral hadrons, photons, muons, and electrons, by combining information from all detector subsystems. All these particles are clustered into jets using the anti-K_T clustering algorithm with distance parameter of 0.5, and are corrected for the effects of pile-up to reduce luminosity dependence on jet energies. To be counted, a jet must have transverse momentum $p_{\mathrm{T}} \geq 30$ GeV, $|\eta| \leq 2.6$ and is required to satisfy requirements designed to reject anomalous nose in the calorimeter detectors. To prevent double counting, jets must be isolated from photons by $\Delta R > 0.4$ to prevent double counting.

3 Background Estimation Methodology

The SUSY signal of interest can be mimicked by SM processes in several ways. The main backgrounds arise from standard model processes with misidentified photons and/or mismeasured $E_{\mathrm{T}}^{\mathrm{miss}}$. The dominant contribution comes from the mis-measurement of $E_{\mathrm{T}}^{\mathrm{miss}}$ in QCD processes such as direct di-photon, photon plus jets, and multijet production, with jets mimicking photons. This will be referred is referred to as the non-true $E_{\mathrm{T}}^{\mathrm{miss}}$ background or as the QCD background. The strategy for determining this background is to use control samples that are kinematically similar to the candidate sample while having no true $E_{\mathrm{T}}^{\mathrm{miss}}$.

The second background comes from events with true missing transverse energy. It is dominated by events with a real or fake photon and a W boson that decays into a neutrino and an electron that is mis-identified as a photon. We refer to this sample as the true $E_{\mathrm{T}}^{\mathrm{miss}}$ or Electroweak (EWK) background. Since all components of this background involve electron-photon misidentification, in order to estimate its contribution to the signal sample, we weight a sample of $e\gamma$ events with $f_{e\to\gamma}/(1-f_{e\to\gamma})$ where $f_{e\to\gamma}$ is the probability to misidentify an electron as a photon. This $e\gamma$ sample has the same requirements imposed on it as the candidate $\gamma\gamma$ sample except a pixel seed is required for one of the EM objects. We also use a sample of ee events where pixel seeds are required on both objects. We measure the p_{T}-dependence of $f_{e\to\gamma}$ by determining the number of $Z \to ee$ events in the ee and $e\gamma$ samples as a function of p_{T}. The overall misidentification rate is $f_{e\to\gamma} = 0.0181 \pm 0.0003\,(\mathrm{stat.}) \pm 0.0009\,(\mathrm{syst.})$ which is used for the di-photon analysis while $f_{e\to\gamma} = 0.011 \pm 0.002\,(\mathrm{stat.}) \pm 0.001\,(\mathrm{syst.})$ for $p_{\mathrm{T}} > 80$ GeV, which is the momentum region relevant for the single-photon analysis and used as misidentification rate in this case.

4 Di-Photon Analysis

In the following we first describe the results of the di-photon analysis and then discuss the search for GGM SUSY production using single-photon events. The di-photon analysis is based on a di-photon trigger with a threshold of 36 GeV (22 GeV) for the leading (sub-leading) photon. To be in a range of full trigger efficiency, the offline analysis requires at least two photons with $E_{\mathrm{T}} > 40$ GeV (25 GeV) for the the leading (sub-leading) photon in the event.

To estimate the QCD background from data, we utilize two different data sets. The first sample contains two fake photons, in what follows referred to as the fake-fake (ff) sample, comprising QCD multijet events. Because of its kinematic similarity to the candidate $\gamma\gamma$ sample, this is used as our main dataset to estimate the QCD background. The second data set contains events with two electrons (ee) with the invariant mass between 70 and 110 GeV, and is dominated by $Z \to ee$ decays. The ee sample is used to study systematic effects in our background estimate. To account for processes contributing to the ee sample with real $E_{\mathrm{T}}^{\mathrm{miss}}$, we subtract sidebands

Table 2: The number of events with $E_{\mathrm{T}}^{\mathrm{miss}} \geq 100$ GeV from $\gamma\gamma$, ff, and $Z \to ee$ as well as the total number of background events with $E_{\mathrm{T}}^{\mathrm{miss}} \geq 100$ GeV using the ff data. The systematic errors quoted apply to the $\geq$ 1-jet sample. We also show the contributions to the errors due to the re-weighting technique and normalization.

Type	MET>100, no jet cut	MET>100, ≥1 jet	Stat Err	Norm Err	Reweight Err	Δ(ee,ff) Err
$\gamma\gamma$	13	11	3.3			
ff QCD background	13.4 ± 13.5	12.9 ± 12.4	3.6	0.0	0.7	11.9
ee QCD background	26.4 ± 13.7	24.7 ± 12.5	3.7	0.0	0.4	11.9
EWK background	5.9 ± 0.3	4.6 ± 0.3	0.3	0.2		
Total background (ff)	19.3 ± 13.5	17.8 ± 12.4				

around the Z peak (i.e. to remove non-peaking contributions like $t\bar{t}$), and use a MC estimate for the ZZ and ZW contributions which contribute within the Z peak (i.e $Z(ee)Z(inv)$).

The fake-fake sample is expected to have a slightly worse $E_{\mathrm{T}}^{\mathrm{miss}}$ resolution with respect to the candidate diphotons by virtue of it containing less isolated EM objects. To address this effect, the difference with respect to the estimate from the *ee* sample, which tends to have more isolated electrons, is used to set the systematic uncertainty on this background estimate. Both separate control samples are re-weighted to reproduce the (di-)photon transverse energy distribution in the data, and, therefore, the transverse energy of hadronic recoil against the photon(s). The $E_{\mathrm{T}}^{\mathrm{miss}}$ distributions in the re-weighted control samples show agreement within uncertainties. The number of events in the ff sample is used to determine the magnitude of the QCD background after normalizing the ff background shape to the di-photon data in the region of low $E_{\mathrm{T}}^{\mathrm{miss}} < 20$ GeV.

As illustration of the validity of the QCD background estimate, in the E_{T} region of 30 to 50 GeV we observe 5310 candidate di-photon events in the sample requiring ≥ 1 jet in the event, while our QCD background estimate in this same region predicts 5512 ± 70 (stat.) ± 669 (syst.). The estimated EWK background is determined with the *ee* and $e\gamma$ samples as described above and is calculated to be much smaller than the QCD background. Other backgrounds such as $Z\gamma\gamma \to \nu\nu\gamma\gamma$, $W\gamma\gamma \to \ell\nu\gamma\gamma$, $t\bar{t}\gamma\gamma$, or $Z\gamma\gamma$ events where the $Z \to \tau\tau$ is followed by a τ decay such as $\tau \to \pi\nu$ or $\tau \to e(\mu)\nu\nu$ have been found to be negligible.

The $E_{\mathrm{T}}^{\mathrm{miss}}$ distribution in the $\gamma\gamma$ sample requiring ≥ 1 jet in the event is represented in Fig. 1 as points with errors bars. The blue shaded area shows the estimated amount of the EWK background. We assume that events with $E_{\mathrm{T}}^{\mathrm{miss}} \leq 20$ GeV have negligible SUSY signal contribution, and scale the $E_{\mathrm{T}}^{\mathrm{miss}}$ distributions of the average QCD prediction so that the integral of the distribution below 20 GeV matches that in the $\gamma\gamma$ sample minus the estimated EWK contribution. The red hatched areas indicate the total background uncertainties.

Following a previous iteration of this analysis [22], Table 2 summarizes the observed number of $\gamma\gamma$ events with $E_{\mathrm{T}}^{\mathrm{miss}} \geq 100$ GeV and the expected backgrounds with the statistical uncertainty and errors due to re-weighting and normalization shown separately. We observe 11 events with $E_{\mathrm{T}}^{\mathrm{miss}} \geq 100$ GeV while the total background expectation is calculated to be 17.8 ± 12.4 events using the ff sample to determine the QCD background plus the EWK background.

To study certain SM processes and to generate SUSY signal events in this search, we use the PYTHIA [27] event generator. In particular, we generate SUSY GGM events in a two-dimensional grid of the gluino, and squark masses for a fixed neutralino mass of 375 GeV,

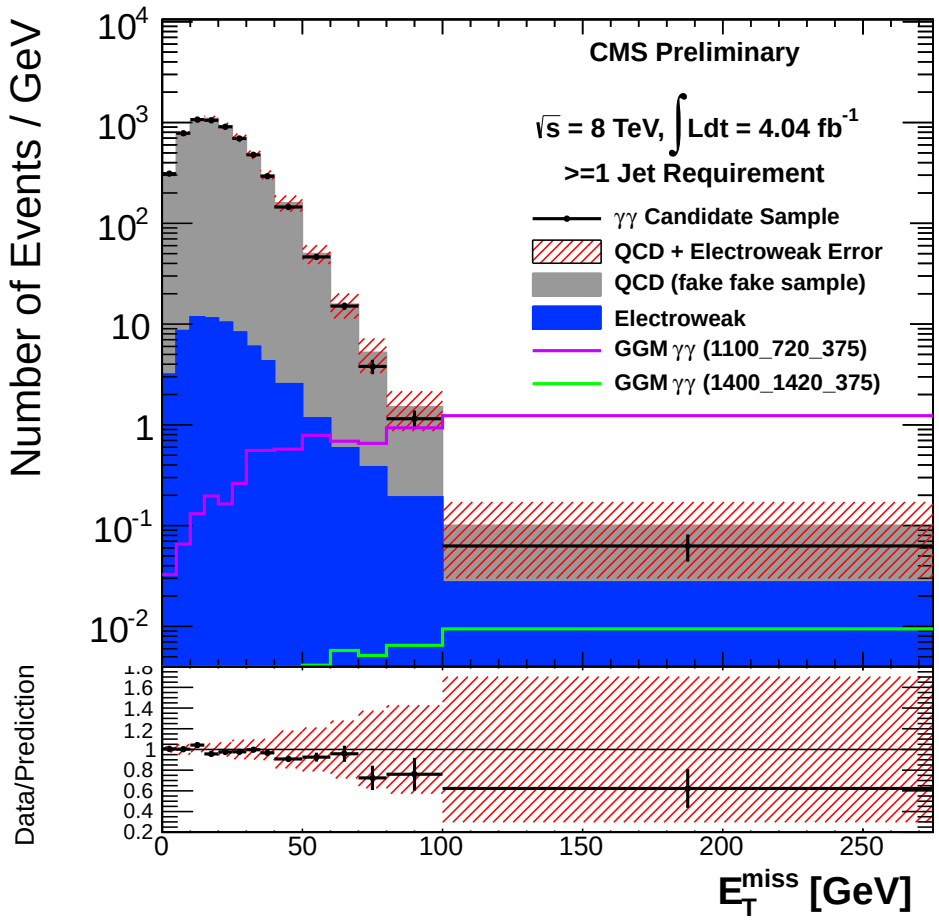

Figure 1: $E_{\mathrm{T}}^{\mathrm{miss}}$ spectrum of $\gamma\gamma$ data compared to QCD prediction together with the small EWK background for events with at least one jet. The red hatched areas indicate the total background uncertainties. Two example GGM points on either side of our exclusion boundary ($m_{\tilde{\mathrm{q}}}/m_{\tilde{\mathrm{g}}}/m_{\tilde{\chi}_1^0}$ in GeV) are also shown.

in the benchmark models in [23]. The neutralino mass value was chosen to be just below the lowest squark and gluino mass in the scan. Squarks are taken to be mass-degenerate. All other SUSY particles are assumed to be heavy. The production cross-section at NLO QCD is calculated for these points using PROSPINO [28] and is dominated by gluino-gluino, gluino-squark, and squark-squark production. The generated events are then passed through the CMS detector simulation program [29] and reconstructed using the same program as for the collision data so that all features of the detector are included in the signal Monte Carlo acceptances.

We determine the efficiency for SUSY events to pass our analysis cuts by applying correction factors derived from the data to the MC simulation of the signal. Since there is no large clean sample of photons in the data, we rely on similarities between the detector response to electrons and photons to extract the photon efficiency. We obtain a scale factor to apply to the photon MC efficiencies by making a ratio of electron efficiency from $Z \to ee$ events that pass all photon ID cuts (except for the pixel match in data) and the corresponding electron MC efficiencies. We apply the obtained scale factor 1.005 ± 0.0001 (stat.) $\pm$ 0.0006 (syst.) to the MC photon efficiencies calculated with MC simulation. Other sources of the larger systematic uncertainties in the signal yield include the error on integrated luminosity (5%), the PDF uncertainty (4-66%) and renormalization scale (4-28%) uncertainty depending on the SUSY sparticle masses.

Using this measurement and the acceptance times efficiency for the SUSY GGM MC and employing the CL_S limit-setting method [30], we determine upper limits for GGM SUSY production. In order to maintain a good signal efficiency, the final signal region for the calculation of exclusion limits is defined with a relatively loose selection criteria requiring $E_{\mathrm{T}}^{\mathrm{miss}} \geq$50 GeV. To still achieve a good sensitivity over a wide range of $E_{\mathrm{T}}^{\mathrm{miss}}$, the limits are calculated in six distinct bins with the following $E_{\mathrm{T}}^{\mathrm{miss}}$ ranges given in GeV: [50,60), [60,80), [80,100), [100,140), [140,180) and [180,∞) and the multi-channel counting experiments are combined into a single limit. We use a log-normal model to incorporate uncertainties on the total background rate, integrated luminosity, and total acceptance times efficiency. The observed 95% C.L. cross-section upper limits vary between 0.002 and 0.012 pb depending on SUSY masses with a typical acceptance of $\sim$ 30% for $E_{\mathrm{T}}^{\mathrm{miss}} > 50$ GeV. The limits are shown at the top of Fig. 2 for squark and gluino masses between 400 and 2000 GeV for a bino-like neutralino of 375 GeV. The value of 375 GeV was chosen to facilitate comparison with previous results [31]. The observed numbers of events, backgrounds and expected signal yields and limits for a sample excluded point is shown in Table 3.

E_T^{miss} bins	50-60 GeV	60-70 GeV	70-80 GeV	80-100 GeV	$>$ 100 GeV
Observed Events	464	151	38	23	11
EW Background	$10.8 \pm 0.5 \pm 0.5$	$5.4 \pm 0.3 \pm 0.3$	$3.5 \pm 0.3 \pm 0.2$	$3.5 \pm 0.3 \pm 0.2$	$4.6 \pm 0.3 \pm 0.2$
QCD Background	$489.9 \pm 22.7 \pm 104.2$	$151.8 \pm 12.7 \pm 42.3$	$48.6 \pm 7.3 \pm 18.2$	$26.4 \pm 5.5 \pm 11.7$	$12.9 \pm 3.7 \pm 11.9$
Signal Yield	3.54 ± 0.65	2.58 ± 0.56	2.92 ± 0.59	8.9 ± 1.0	275.4 ± 5.8
Expected Limit	11.234 pb	6.756 pb	2.066 pb	0.496 pb	0.011 pb
Observed Limit	9.908 pb	6.489 pb	1.716 pb	0.404 pb	0.0074 pb
Combined Expected Limit			0.0095 pb		
Combined Observed Limit			0.0069 pb		
Signal Cross Section			0.258 pb		

Table 3: Example of inputs for limit setting for an excluded model point (jet required, m_{squark} = 900 GeV, m_{gluino} = 920 GeV, m_{bino} = 375 GeV). The combined limits from all 5 bins is also shown.

Since the physical neutralinos and charginos are an admixture of gaugino eigenstates, we have studied two different models of gaugino mixing: one in which the bino mass scale is much lighter than the wino mass scale, and one in which the converse is true. In the "bino-like"

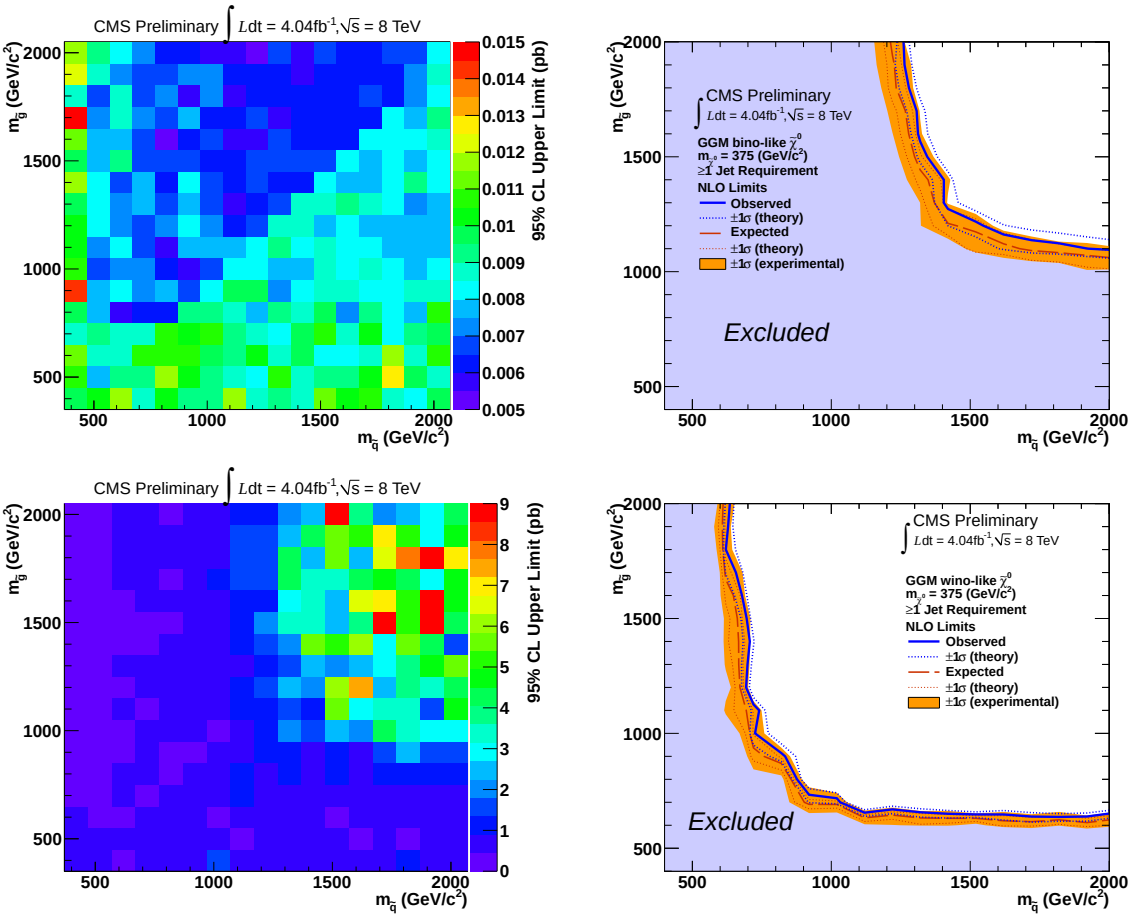

Figure 2: 95% C.L. observed upper limits on the signal cross section (left) and corresponding exclusion contours (right) in gluino-squark mass space for bino- (top) and wino-like (bottom) neutralino for the di-photon analysis. The shaded uncertainty band around the exclusion contours correspond to the NLO renormalization and PDF uncertainties of the signal cross section.

scenario where production of two photons dominate, the acceptance is higher, leading to the more stringent exclusion limits, shown in the top of figure 2. The corresponding limits for a wino-like neutralino are at the bottom of Fig. 2. These are an improvement over the 2011 results by about 150 GeV in the squark mass plane, and about 100 GeV in the gluino mass plane. In the wino-like case the acceptance drops to $\sim 1\%$, leading to a much less stringent cross section cross section limit of ~ 0.01 pb. This limit is also improved over the 2011 result.

5 Single Photon Analysis

The single-photon analysis is based on a trigger requiring the presence of one photon with $E_T > 70$ GeV and the scalar sum (H_T) of the transverse energies of all jets with in the event with $p_T > 40$ GeV and $|\eta| < 3.0$ to be greater than 400 GeV. This analysis is based on the same data set as the di-photon analysis previously described. The offline analysis requires $H_T \geq 450$ GeV for the H_T trigger to become fully efficient, and requires at least one tight photon with $E_T > 80$ GeV within $|\eta| < 1.4442$. The tight photon requirements are described in Section 2. In addition, we require ≥ 2 jets with $p_T \geq 30$ GeV and $|\eta| \leq 2.6$.

The QCD background in the single-photon analysis is a composition of direct photon-jet pro-

duction and of QCD multijet production, where one jet is misidentified as a photon. The shape of the $E_{\mathrm{T}}^{\mathrm{miss}}$ distribution, including the non-Gaussian tails, is similar for both background contributions, as the event topology is very similar between the two. Therefore, these two QCD contributions are estimated together from the same data control sample. The control sample is selected by applying the same signal selection requirements, except that the photon candidate is required to fail the tight selection criteria but satisfy a looser isolation requirement. We refer to such photon candidates as γ_{jet}, whose identification is by definition orthogonal to the photon ID criteria in the signal selection. The control sample has to be weighted, to correct for the different p_{T} spectra of γ_{jet} and tight photon objects in the control and signal samples, respectively. The weights are determined in a signal-depleted region with $E_{\mathrm{T}}^{\mathrm{miss}} < 100$ GeV and the weight vs. photon candidate E_{T} is taken from a histogram in bins of p_{T}.

The strategy to model the electroweak background contribution, which is much smaller than the QCD background, is similar to that in the di-photon analysis, as described above. The dominant contributions are from $\mathrm{t\bar{t}}$ production or events with W or Z bosons with one or more neutrinos in the final state. Additional backgrounds can occur due to initial state radiation (ISR) and final state radiation (FSR) of photons. ISR and FSR in events with electrons in the final state are already covered by the electroweak background prediction from data and the remaining contributions from SM process mainly from W, Z and $t\bar{t}$ events are very small and directly taken from Monte Carlo simulation with a conservative systematic uncertainty of 100%. These backgrounds are summarized in Table 4, along with sample results for the limits described below.

The combined background prediction, the observed data and two GGM benchmark signal samples, one excluded and one not excluded, are shown in Fig. 3. The expected and observed event yields are summarized in Table 4. No excess beyond standard model predictions is observed.

The final signal region for the calculation of exclusion limits is defined with a relatively loose selection criteria requiring $E_{\mathrm{T}}^{\mathrm{miss}} \geq 100$ GeV. To still achieve a good sensitivity, the limits are calculated in six distinct bins with the following $E_{\mathrm{T}}^{\mathrm{miss}}$ ranges in GeV: [100,120), [120,160), [160,200), [200,270), [270,350) and [350,∞). In the same way as described for the di-photon analysis above, the multi-channel counting experiments are combined into a single limit. We again use the $\mathrm{CL_S}$ method to determine 95% confidence level (C.L.) upper limits for the squark versus gluino mass plane from 400 to 2000 GeV in squark and gluino mass with the neutralino mass set again at 375 GeV to facilitate comparison with previous results [22].

A possible contamination of signal in the background sample used for the background estimation has been studied and is considered in the limit calculation. For this purpose the expected amount of SUSY GGM events in the background estimation has been subtracted from the number of observed signal events, lowering the acceptance times efficiency by a few percent for each point. The resulting limits, after subtraction of the signal contamination, are shown in Fig. 4. For the bino-like scenario the resulting upper limit cross section is of order 0.01 pb with a typical acceptance of $\sim$ 77% for $E_{\mathrm{T}}^{\mathrm{miss}} > 100$ GeV. For the wino like scenario the acceptance drops to $\sim$ 7%, leading to an upper limit cross section of $\sim$ 0.08 pb. The expected limit contours improve by about 100 GeV in the bino-like case, and about 50 GeV in the wino-like scenario over our 2011 results.

6 Summary

In summary, we have searched for evidence of GGM SUSY production in di-photon and single-photon events using the $E_{\mathrm{T}}^{\mathrm{miss}}$ spectrum beyond 100 GeV. This search is based on 2012 CMS

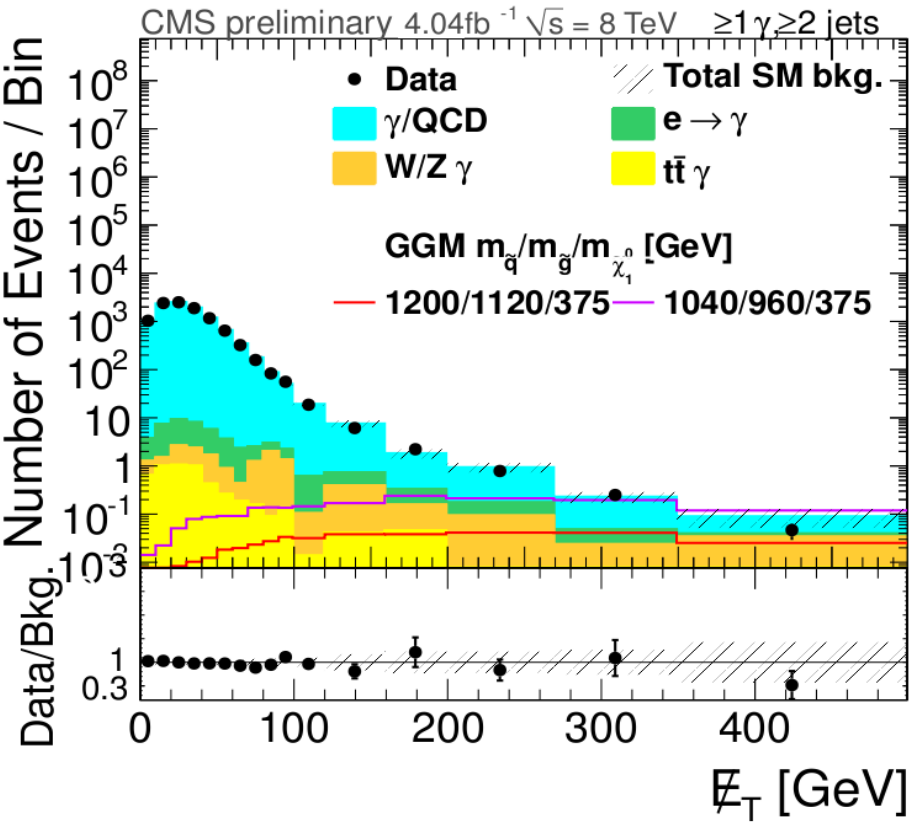

Figure 3: Total standard model background prediction compared to the number of single-photon events, including two GGM benchmark signal benchmark points as examples where masses ($m_{\tilde{q}}/m_{\tilde{g}}/m_{\tilde{\chi}_1^0}$) are given in GeV.

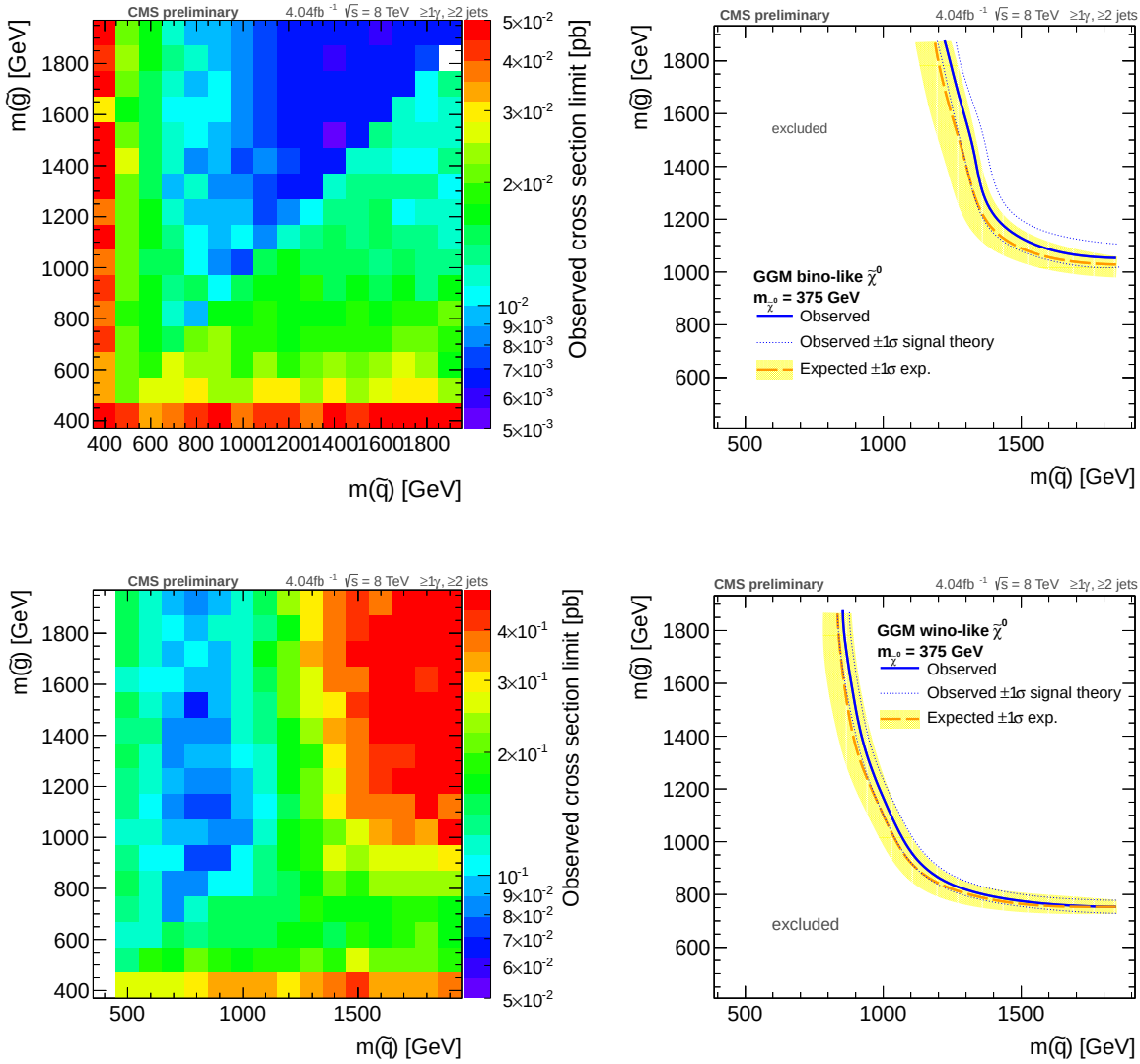

Figure 4: 95% C.L. observed upper limits on the signal cross section (left) and corresponding exclusion contours (right) in gluino-squark mass space for bino- (top) and wino-like (bottom) neutralino for the single photon analysis. The shaded uncertainty band around the exclusion contours correspond to the NLO renormalization and PDF uncertainties of the signal cross section.

Table 4: Observed and expected event yields, acceptance $\times$ efficiency ($A \times \varepsilon$) and obtained limits for each exclusive signal bin for a sample GGM point ($m_{\tilde{\chi}_1^0} = 375$ GeV (bino-like), $m_{\tilde{g}} = 800$ GeV, $m_{\tilde{q}} = 720$ GeV) and the ≥ 2 jet selection. The total combined observed (expected) 95%CL limits on the signal-cross section are 0.012 pb (0.013 pb). The NLO signal cross-section for this point is 0.979 pb.

$E_{\mathrm{T}}^{\mathrm{miss}}$ bins [GeV]	Bin 0 [100,120)	Bin 1 [120,160)	Bin 2 [160,200)
QCD	394±41	267±51	60±17
EWK	10.6±2.9	13.4±3.7	6.9±1.9
ISR/FSR	2.0±1.2	13.8±8.5	5.6±3.5
Background	406±42	294±52	73±17
Data	392	239	89
Signal	113±8	281±15	277±15
Signal contamination	19.44	38.28	50.15
Acceptance [%]	2.9	7.1	7.1
Exp. limit [pb]	0.802	0.270	0.183
Obs. limit [pb]	0.733	0.218	0.217
Exp. limit [events]	92.1	77.4	51.8
Obs. limit [events]	84.2	62.5	61.5

$E_{\mathrm{T}}^{\mathrm{miss}}$ bins [GeV]	Bin 3 [200,270)	Bin 4 [270,350)	Bin 5 [350,∞)
QCD	53.7±14.6	14.5±4.7	8.9±4.3
EWK	5.6±1.6	1.9±0.5	1.0±0.3
ISR/FSR	5.9±3.7	1.7±1.3	4.7±4.7
Background	65.2±15.1	18.2±4.9	14.6±6.4
Data	55	20	8
Signal	538±25	529±25	640±29
Signal contamination	86.71	91.53	127.71
Acceptance [%]	13.7	13.5	16.3
Exp. limit [pb]	0.055	0.027	0.019
Obs. limit [pb]	0.051	0.031	0.012
Exp. limit [events]	30.0	14.3	12.2
Obs. limit [events]	28.2	16.8	8.0

data comprising 4.04 fb^{-1} of pp collisions at $\sqrt{s} = 8$ TeV. We find no evidence of GGM SUSY production and set upper limits for a range of parameters in that model. For the single and di-photon analyses we have defined 95% C.L. exclusion regions for the production cross sections in the GGM SUSY parameter space of squark and gluino masses of order 0.01 pb (0.1 pb) for the bino- (wino-) like scenarios. These limits are the most stringent placed on these scenarios to date.

References

[1] P. Fayet, "Mixing Between Gravitational and Weak Interactions Through the Massive Gravitino", *Phys. Lett.* **B70** (1977) 461, doi:10.1016/0370-2693(77)90414-2.

[2] H. Baer, M. Brhlik, C. H. Chen et al., "Signals for the Minimal Gauge-Mediated

Supersymmetry Breaking Model at the Fermilab Tevatron Collider", *Phys. Rev.* **D55** (1997) 4463, doi:10.1103/PhysRevD.55.4463.

[3] H. Baer, P. G. Mercadante, X. Tata et al., "Reach of Tevatron Upgrades in Gauge-Mediated Supersymmetry Breaking Models", *Phys. Rev.* **D60** (1999) 055001, doi:10.1103/PhysRevD.60.055001.

[4] S. Dimopoulos, S. Thomas, and J. D. Wells, "Sparticle Spectroscopy and Electroweak Symmetry Breaking with Gauge-Mediated Supersymmetry Breaking", *Nucl. Phys.* **B488** (1997) 39, doi:10.1016/S0550-3213(97)00030-8.

[5] J. R. Ellis, J. L. Lopez, and D. V. Nanopoulos, "Analysis of LEP Constraints on Supersymmetric Models with a Light Gravitino", *Phys. Lett.* **B394** (1997) 354, doi:10.1016/S0370-2693(97)00019-1.

[6] M. Dine, A. Nelson, Y. Nir et al., "New Tools for Low Energy Dynamical Supersymmetry Breaking", *Phys. Rev.* **D53** (1996) 2658, doi:10.1103/PhysRevD.53.2658.

[7] G. F. Giudice and R. Rattazzi, "Gauge-Mediated Supersymmetry Breaking", in *Perspectives on Supersymmetry*, p. 355. World Scientific, Singapore, 1998.

[8] P. Meade, N. Seiberg, and D. Shih, "General Gauge Mediation", *Prog. Theor. Phys. Suppl.* **177** (2009) 143, doi:10.1143/PTPS.177.143.

[9] M. Buican, P. Meade, N. Seiberg et al., "Exploring General Gauge Mediation", *JHEP* **0903** (2009) 016, doi:10.1088/1126-6708/2009/03/016.

[10] G. R. Farrar and P. Fayet, "Phenomenology of the Production, Decay, and Detection of New Hadronic States Associated with Supersymmetry", *Phys. Lett.* **B76** (1978) 575, doi:10.1016/0370-2693(78)90858-4.

[11] CMS Collaboration, "Search for New Physics with Long-Lived Particles Decaying to Photons and Missing Energy", CMS Physics Analysis Summary CMS-PAS-EXO-11-067, (2011).

[12] ATLAS Collaboration, "Search for Diphoton Events with Large Missing Transverse Energy with 36 pb^{-1} of 7 TeV Proton-Proton Collision Data with the ATLAS Detector", *Eur. Phys. J.* **C71** (2011) 1744, doi:10.1140/epjc/s10052-011-1744-9, arXiv:1107.0561.

[13] ATLAS Collaboration, "Search for Diphoton Events with Large Missing Transverse Momentum in 1 $fb^{-}1$ of 7 TeV Proton-Proton Collision Data with the ATLAS Detector", *Phys. Lett.* **B710** (2012) 519, arXiv:1111.4116.

[14] CMS Collaboration, "Search for Supersymmetry in pp Collisions at sqrt(s) = 7 TeV in Events with Two Photons and Missing Transverse Energy", *Phys. Rev. Lett.* **106** (2011) 211802, doi:10.1103/PhysRevLett.106.211802.

[15] T. Aaltonen et al., "Search for Supersymmetry with Gauge-Mediated Breaking in Diphoton Events with Missing Transverse Energy at CDF II", *Phys. Rev. Lett.* **104** (2010) 011801, doi:10.1103/PhysRevLett.104.011801.

[16] V. M. Abazov et al., "Search for Diphoton Events with Large Missing Transverse Energy in 6.3 fb^{-1} of $p\bar{p}$ Collisions at $\sqrt{s}$ = 1.96 TeV", *Phys. Rev. Lett.* **105** (2010) 221802, doi:10.1103/PhysRevLett.105.221802.

[17] A. Heister et al., "Search for Gauge Mediated SUSY Breaking Topologies in e^+e^- Collisions at Centre-of-Mass Energies up to 209 GeV", *Eur. Phys. J.* **C25** (2002) 339, doi:10.1007/s10052-002-1005-z.

[18] J. Abdallah et al., "Photon Events with Missing Energy in e^+e^- Collisions at $\sqrt{(s)} = 130$ to 209 GeV", *Eur. Phys. J.* **C38** (2005) 395, doi:10.1140/epjc/s2004-02051-8.

[19] P. Achard et al., "Single- and Multi-Photon Events with Missing Energy in e^+e^- Collisions at LEP", *Phys. Lett.* **B587** (2004) 16, doi:10.1016/j.physletb.2004.01.010.

[20] G. Abbiendi et al., "Search for Gauge-Mediated Supersymmetry Breaking Topologies in e^+e^- Collisions at LEP2", *Eur. Phys. J.* **C46** (2006) 307, doi:10.1140/epjc/s2006-02524-8.

[21] A. Aktas et al., "Search for Light Gravitinos in Events with Photons and Missing Transverse Momentum at HERA", *Phys. Lett.* **B616** (2005) 31, doi:10.1016/j.physletb.2005.04.038.

[22] CMS Collaboration, "Search for Supersymmetry in Events with Photons, Jets and Missing Energy", CMS Physics Analysis Summary CMS-PAS-SUS-12-001, (2012).

[23] LHC New Physics Working Group, "Simplified Models for LHC New Physics Searches", (2010). See http://www.lhcnewphysics.org/photons.

[24] CMS Collaboration, "The CMS experiment at the CERN LHC", *JINST* **03** (2008) S08004, doi:10.1088/1748-0221/3/08/S08004.

[25] P. Adzic et al., "Energy resolution of the barrel of the CMS electromagnetic calorimeter", *JINST* **2** (2007) P04004, doi:10.1088/1748-0221/2/04/P04004.

[26] CMS Collaboration, "Particle–Flow Event Reconstruction in CMS and Performance for Jets, Taus, and $E_{\mathrm{T}}^{\mathrm{miss}}$", *CMS Physics Analysis Summary* **CMS-PAS-PFT-09-001** (2009).

[27] T. Sjostrand, S. Mrenna, and P. Z. Skands, "PYTHIA 6.4 Physics and Manual", *JHEP* **0605** (2006) 026, doi:10.1088/1126-6708/2006/05/026, arXiv:hep-ph/0603175.

[28] W. Beenakker, R. Höpker, M. Spira et al., "Squark and Gluino Production at Hadron Colliders", *Nucl. Phys.* **B492** (1997) 51, doi:10.1016/S0550-3213(97)80084-9.

[29] GEANT4 Collaboration, "GEANT4: A Simulation toolkit", *Nucl.Instrum.Meth.* **A506** (2003) 250–303, doi:10.1016/S0168-9002(03)01368-8.

[30] Particle Data Group Collaboration, "Review of particle physics", *J. Phys.* **G37** (2010) 075021, doi:10.1088/0954-3899/37/7A/075021.

[31] CMS Collaboration, "Search for Supersymmetry in Events with Photons, Jets and Missing Energy", CMS Physics Analysis Summary CMS-PAS-SUS-11-009, (2011).